

Desulfurization Behavior of Incoloy[®] 825 Superalloy by CaO-Al₂O₃-MgO-TiO₂ Slag



JIN HYUNG CHO, JOHAN MARTINSSON, DU SICHEN, and JOO HYUN PARK

Ni-based superalloy, which has excellent high-temperature strength and corrosion resistance, is mainly used in aviation materials, high-performance internal combustion engines, and turbines for thermal and nuclear power generation. For this reason, refining the impurities in Ni-based superalloys is a very important technical task. Nevertheless, the original technology for the melting and refining of Ni-based superalloys is still insufficient. Therefore, in this study, the effect of the CaO-Al₂O₃-MgO-TiO₂ slag on the removal efficiency of an impurity element sulfur in Incoloy[®] 825 superalloy, one of the representative Ni-based superalloys, was investigated. The desulfurization behavior according to the change of TiO₂ content and CaO/Al₂O₃ (=C/A, basicity) ratio as experimental variables was observed at 1773 K (1500 °C). Although the TiO₂ content in the slag increases to 15 mass pct, the mass transfer coefficient of sulfur in molten alloy showed a constant value. Alternatively, under the condition of C/A > 1.0 of slag, the mass transfer coefficient of sulfur showed a constant value, whereas under the condition of C/A < 1.0, the mass transfer coefficient of sulfur greatly decreased as CaO decreased. Hence, in the desulfurization of Incoloy[®] 825 superalloy using the CaO-Al₂O₃-MgO-TiO₂ slag, the TiO₂ content in the slag does not have a considerable effect on the desulfurization rate and desulfurization mechanism (metal phase mass transfer controlled regime), but the basicity of the slag has a significant effect on desulfurization mechanism. When the slag basicity decreases below the critical level, *i.e.*, C/A < 1.0, which is corresponding to sulfur distribution ratio, $L_s < 200$, it was confirmed that the desulfurization mechanism shifts from the metal phase mass transfer-controlled regime to the slag phase mass transfer-controlled regime due to the variation in the physicochemical properties of the slag such as viscosity and sulfide capacity. In addition, the different desulfurization rates between steel and Ni alloy melts were discussed by employing the diffusivity of sulfur in both systems.

<https://doi.org/10.1007/s11663-021-02338-9>

© The Author(s) 2021

I. INTRODUCTION

NICKEL-BASED superalloys usually have high strength and corrosion resistance at severe environment with high temperatures. Due to this property, they have been used as aviation material, high-performance internal combustion engine, thermal power, and nuclear

power turbine. However, because the impurities, such as sulfur, phosphorous, oxygen, and nitrogen can react with the host metal or other alloying elements to form precipitates that have detrimental effects on physical properties of the final product, the removal of these impurity elements is highly important for use of Ni-based alloys in the above applications.^[1,2] In particular, sulfur adversely affects tensile ductility, stress rupture life, and crack propagation resistance in Ni-based superalloys.^[2,3]

Since the 1970s, in order to improve the quality and performance of Ni-based superalloys, many studies have been conducted to remove sulfur from alloy melts.^[4-6] Utada *et al.*^[7] reported the ‘direct and complete recycling,’ which is the method that cast a single crystal alloy using a CaO crucible and adjusting the composition of the melt. Degawa and Ototani^[8] also investigated desulfurization behavior of Ni-based superalloy, Inconel[®] 738 using calcia (CaO) refractory. They concluded that calcia refractory is very effective not only in desulfurization but also in deoxidation as well as

JIN HYUNG CHO is with the Department of Materials Science and Chemical Engineering, Hanyang University, Ansan, 15588, Korea. JOHAN MARTINSSON is with the Business Area of Metallurgy, Swerim AB, Kista 16440, Sweden and also with Department of Materials Science and Engineering, KTH Royal Institute of Technology, Stockholm 11428, Sweden. DU SICHEN is with the Department of Materials Science and Engineering, KTH Royal Institute of Technology. JOO HYUN PARK is with the Department of Materials Science and Chemical Engineering, Hanyang University and also with the Department of Materials Science and Engineering, KTH Royal Institute of Technology, Stockholm. Contact e-mail: basicity@hanyang.ac.kr

Manuscript submitted May 31, 2021; accepted September 19, 2021.

Article published online October 15, 2021.

nitrogen removal process. Kishimoto *et al.*^[9] reported the desulfurization model in molten Ni-based superalloy by using solid CaO rod and calculated the effective sulfur diffusivity in molten Ni-based superalloy. Also, they found that CaO and Al₂O₃ generate solid calcium aluminates, which capture CaS to remove S from the melt at 1673 K (1400 °C), while CaO and Al₂O₃ form the solid–liquid coexisting calcium aluminates, which capture CaS and penetrate the particle boundaries of the CaO rod to remove S from the melt at 1773 K and 1873 K (1500 °C and 1600 °C).^[10] Moreover, they suggested that the rate-determining process of the desulfurization reaction is sulfur diffusion in the generated calcium aluminates layer at any temperature.

Refining of Ni-based superalloys is typically performed by vacuum induction melting (VIM) and electroslag remelting (ESR) in industry. Zhang *et al.*^[11] investigated the desulfurization behavior of Ni-based superalloy, in which Al was added as desulfurizer using VIM method. Niu and Hu^[12] reported the nitrogen removal mechanism in Ni-based superalloy during VIM and calculated the activity coefficient of N ($f_N = 0.714$). On the other hand, the ESR process, which is a method of refining metals employing a molten slag that is heated by electrical resistance, has been adopted as a refining process to produce ultra-clean Ni-based alloys.^[13] Eissa and El-Mohammadi^[14] confirmed that high degree of desulfurization of steels can be attained by using the 70CaF₂-15CaO-15Al₂O₃ (mass pct) ESR slag system. Yang and Park^[15] studied the ESR slag design to control Al and Ti contents in the Ni-based alloy using ESR process. Duan *et al.*^[16] reported that increasing TiO₂ content in the ESR slag decreased the desulfurization efficiency of Inconel[®] 718 alloy.

Alternatively, Kellner *et al.*^[17] investigated the evolution of non-metallic inclusions from FeTi70 ferroalloy and Incoloy[®] 825 superalloy melt through the high-temperature experiments, which have similarity with ladle refining process in steel industry. Nevertheless, there are few studies on ladle refining concept of Ni-based superalloys. Comprehensively, although the special melting and refining processes such as VIM and ESR produce high-quality alloys, the process cost is generally higher than commercial ladle refining technology.

Therefore, in the present study, along with the pursuit of reducing the production cost due to the VIM and ESR processes, the applicability of the desulfurization of Ni-based superalloy using CaO-based ladle slag was investigated. The desulfurization behavior of Ni-based superalloy using the CaO-Al₂O₃-MgO-TiO₂ slags with different TiO₂ contents and different CaO/Al₂O₃ ratios on the desulfurization kinetics of Incoloy[®] 825 superalloy was conducted at 1773 K (1500 °C).

II. EXPERIMENTAL PROCEDURE

The experiments were performed using a high-frequency induction furnace (Figure 1). The quartz reaction chamber was initially evacuated prior to carrying

out the experiments and the chamber was thereafter filled with a purified Ar-3 pct H₂ gas mixture. Impurities in the Ar-3 pct H₂ gas mixture were removed by passing the gas through Drierite[®] (W.A Hammond Drierite Co. Ltd., Xenia, OH), silica gel, soda lime, and Mg turnings at 773 K (500 °C).

The Incoloy[®] 825 superalloy (500 g) was put into a fused MgO crucible (51 mm inner diameter, 60 mm outer diameter, 100 mm height) with a graphite heater, which was surrounded by insulation. The composition of Incoloy[®] 825 superalloy used in the present experiments is listed in Table I. The experimental temperature was 1773[± 2] K (1500[± 2] °C), which was regulated using a proportional–integral–differential controller and a B-type (Pt-30Rh/Pt-6Rh, mass pct) thermocouple.

After the temperature stabilization was confirmed, slag (50 g), which was prepared using a vertical resistance furnace with a mixture of reagent grade CaO, calcined from CaCO₃ at 1273 K (1000 °C), Al₂O₃, MgO, and TiO₂, was injected through the quartz tube. The compositions of the pre-fused slags are listed in Table II and are plotted in the CaO-Al₂O₃-TiO₂-5 pct MgO phase diagram (Figure 2) with iso-activity CaO contours, which were constructed from FactSageTM7.3 calculations.

In situ suction sampling and quenching were employed to obtain alloy and slag samples during the metal–slag reactions at 1773 K (1500 °C) at various time intervals (0, 5, 10, 20, 30, 60 minutes). The sulfur content in the slag and metal samples was measured using a combustion analyzer (CS 800, ELTRA). By using an inductively coupled plasma-atomic emission spectrometry (ICP-AES, ACROS, SPECTRO), the alloy composition was obtained. The experimental results according to the slag compositions are listed in Table II. The saturation level of MgO in the present slag system was calculated to (MgO)_{sat} = 6–8 mass pct using FactSageTM7.3 software with FToxid database and was experimentally confirmed that the slag composition was not seriously different from the initial one within the analytical error range, *i.e.*, ± 2 pct. Hence, the slag composition is expressed as initial one in the present study. The equilibrium sulfur content and sulfur distribution ratio in each condition were obtained in the separate experiments, which are described elsewhere.^[18]

In the present slag system, the ionic speciation of titanium oxide, which is dependent on the oxygen chemical potential, was confirmed by employing an X-ray photoelectron spectroscopy (XPS, K-alpha (mono); Thermo UK) analysis with quenched slag samples. From XPS spectra for Ti 2p shown in Figure 3, it was confirmed that the oxidation state of Ti was Ti⁴⁺ in the present CaO-Al₂O₃-TiO₂-MgO slag system from the observation of Ti⁴⁺ peaks (458.5 eV). The representative binding energy is shown in Table III.^[15,19] Hence, through the 458.5 eV peak in Figure 3, it can be reasonably assumed that titanium is mainly stabilized as TiO₂ in the present slag system under the present experimental conditions.

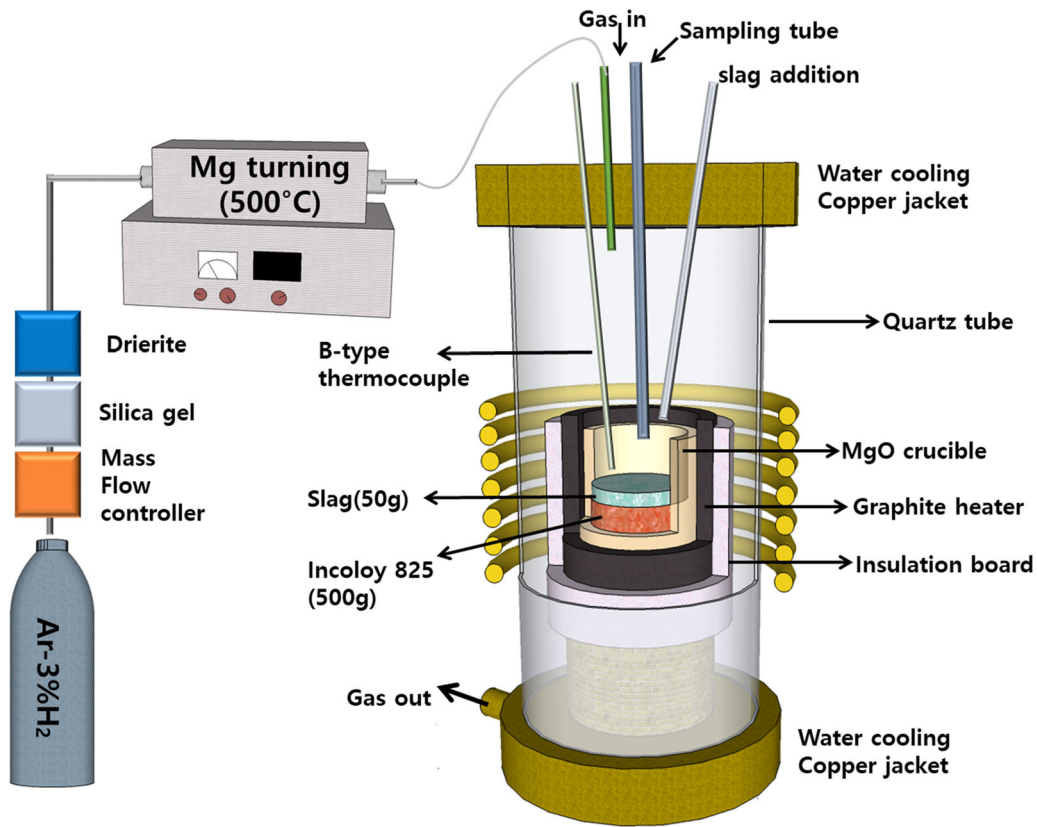


Fig. 1—Schematic diagram of the experimental apparatus.

Table I. Composition of Incoloy[®] 825 Superalloy (Mass Pct)

Ni	Fe	Cr	Mo	Cu	Ti	C	Mn	S	Si	Al
40.8	22.5	29.2	3.5	1.9	0.43	0.04	0.5	0.145	0.2	0.07

Table II. Composition of Slag and Experimental Results in the Present Study

Variable	Chemical Composition (Mass Pct)					L_S
	CaO	Al ₂ O ₃	MgO	TiO ₂	[pct S] _{eq}	
TiO ₂ (Mass Pct)						
0	51.5	43.0	5.5	0.0	0.0040(± 0.0004)	400(± 70)
5	51.0	38.0	6.0	5.0	0.0027(± 0.0004)	570(± 95)
10	50.5	33.0	6.5	10.0	0.0026(± 0.0003)	540(± 50)
15	50.0	28.0	7.0	15.0	0.0026(± 0.0003)	585(± 65)
CaO/Al ₂ O ₃ (Mass Ratio)						
0.62	34.0	55.0	6.0	5.0	0.0157(± 0.0026)	40(± 8)
0.70	36.5	52.5	6.0	5.0	0.0075(± 0.0009)	110(± 25)
0.96	43.5	45.5	6.0	5.0	0.0054(± 0.0008)	280(± 40)
1.34	51.0	38.0	6.0	5.0	0.0027(± 0.0004)	570(± 95)

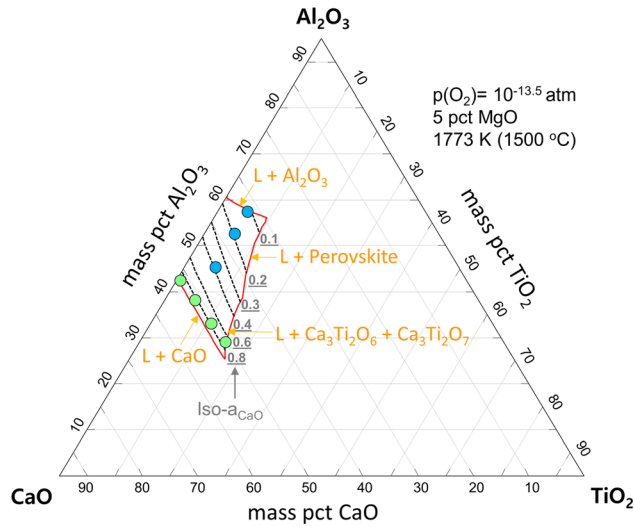


Fig. 2—Experimental compositions of the present study represented in the CaO-TiO₂-Al₂O₃-5 pct MgO phase diagram with iso-*a*_{CaO} lines, calculated by FactSageTM 7.3.

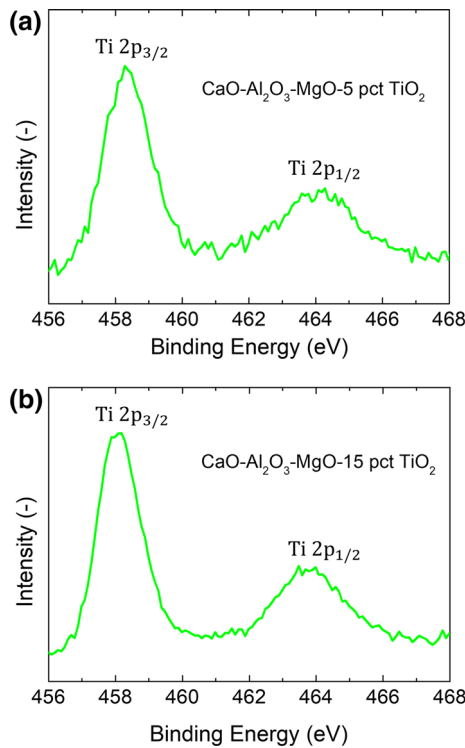


Fig. 3—X-ray photoelectron spectroscopy spectra of quenched slag samples depending on the content of titanium oxide: (a) TiO₂ = 5 mass pct and (b) TiO₂ = 15 mass pct.

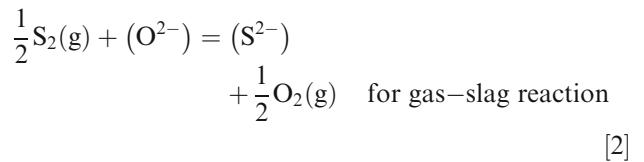
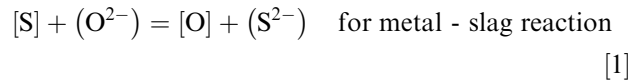
Table III. Binding Energy of Titanium Oxides at Different Valances^[15,19]

	Ti ²⁺	Ti ³⁺	Ti ⁴⁺
Binding Energy	455.0 eV	457.0 eV	458.5 eV

III. RESULTS AND DISCUSSION

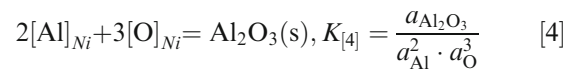
A. Thermodynamics of Sulfur Removal from Incoloy[®] 825 Superalloy: Sulfide Capacity and Sulfur Distribution Ratio

The equilibrium S distribution ratio ($= L_s = (\text{mass pct S}) / [\text{mass pct S}]$) between metal and slag is used to evaluate the desulfurization efficiency regarding thermodynamics in iron- and steelmaking processes. In order to investigate the influence of sulfide capacity ($= C_{S^{2-}}$) and desulfurization conditions on L_s , the sulfide capacity of the slag was calculated from Eq. [3] deduced from desulfurization reactions, Eqs. [1] and [2].



$$\log C_{S^{2-}} = \log L_s + \log a_O - \log f_S \quad [3]$$

here a_O is the activity of oxygen in molten alloy, determined by the Al-Al₂O₃ equilibrium reaction according to Eq. [4].^[5]



$$\log K_{[4]} = \frac{60,790}{T} - 18.8, \quad [5]$$

and f_S is the activity coefficient of S in molten Incoloy[®] 825 superalloy, which was assumed to be unity due to scarcity of thermodynamic data, e.g., interaction parameters for all solute elements, in Ni-based melts. The calculated activity of oxygen in molten alloy and that of Al₂O₃ in the slag are listed in Table IV.

The sulfide capacity $C_{S^{2-}}$ was also calculated using the FactSageTM 7.3 software,^[20,21] a commercial thermochemical computing package which has been widely used to obtain the equilibria of multicomponent, and multiphase metallurgical systems.^[22-31] The effect of the different TiO₂ content and C/A ratio on $C_{S^{2-}}$ can be compared and the calculation results are plotted as iso-capacity contours in Figure 4. It can be easily found that the iso-capacity contours exhibit nearly the same tendency with the iso- a_{CaO} contour in the present slag system: i) Sulfide capacity strongly dependent on the CaO content, ii) Sulfide capacity contours are parallel to the CaO saturation liquidus line, iii) Effect of TiO₂ content on sulfide capacity is less significant than that of

Table IV. Activity of Oxygen and Alumina Used for Capacity Calculation in the Present Study

Variable	Activity	
	$\log a_{\text{O}}$	$\log a_{\text{Al}_2\text{O}_3}^*$
TiO ₂ (Mass Pct)		
0	- 5.17	- 1.70
5	- 5.20	- 1.68
10	- 5.14	- 1.70
15	- 5.08	- 1.61
CaO/Al ₂ O ₃ (Mass Ratio)		
1.34	- 5.20	- 1.68
0.96	- 4.95	- 1.09
0.70	- 4.78	- 0.63
0.62	- 4.71	- 0.51

* $a_{\text{Al}_2\text{O}_3}$ was calculated by FactSageTM7.3 software using FToxid DB.

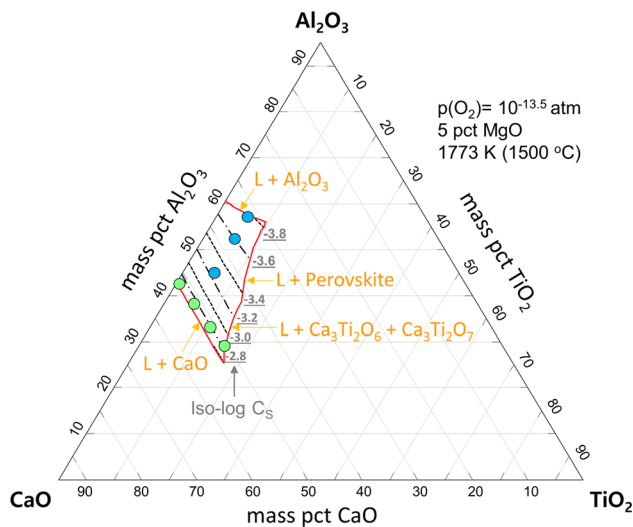


Fig. 4—Iso-sulfide capacity contours in the CaO-Al₂O₃-5 pct MgO-TiO₂ slag system at 1773 K (1500 °C), calculated from FactSageTM7.3.

CaO, and iv) Sulfide capacity slightly decreases with increasing TiO₂ content at a given C/A ratio (but not significant).

Moreover, for the calculation of sulfide capacity with various TiO₂ contents and C/A ratios, a relationship between sulfide capacity and theoretical optical basicity reported by several authors was employed. Duffy and Ingram^[32–34] defined the optical basicity as the ability of an oxygen anion to provide negative charge to the oxide melts. The optical basicity of slags can be calculated from Eq. [6]:

$$\Lambda_{\text{melt}} = \frac{\sum x_i n_i \Lambda_i}{\sum x_i n_i}, \quad [6]$$

where x_i is mole fraction of oxide component i , n_i is the number of oxygen in component of each oxide i , and Λ_i is optical basicity of pure oxide component i ,

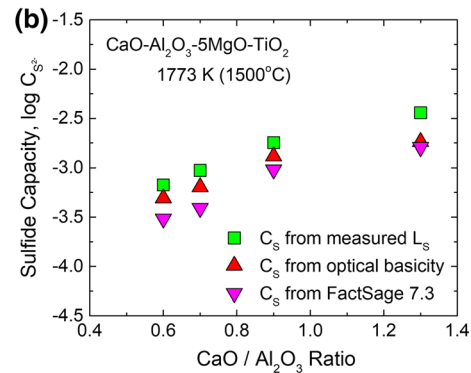
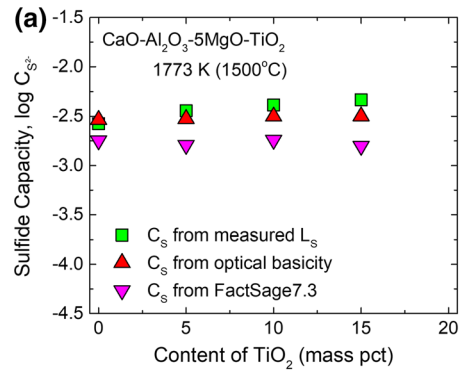


Fig. 5—Sulfide capacity of the CaO-Al₂O₃-5 pct MgO-TiO₂ slags as a function of various (a) TiO₂ contents and (b) CaO/Al₂O₃ ratios at 1773 K (1500 °C).

i.e., $\Lambda_{\text{CaO}} = 1.0$, $\Lambda_{\text{TiO}_2} = 0.61$, $\Lambda_{\text{Al}_2\text{O}_3} = 0.60$, and $\Lambda_{\text{MgO}} = 0.78$. Sosinsky and Sommerville^[35] obtained a correlation between sulfide capacity and optical basicity such as Eq. [7] at temperatures from 1673 K (1400 °C) to 1973 K (1700 °C):

$$\log C_{\text{S}^{2-}} = \frac{22,690 - 54,650\Lambda_{\text{melt}}}{T} + 43.6\Lambda_{\text{melt}} - 25.2. \quad [7]$$

The sulfide capacity calculated from FactSageTM7.3 software, experimental results, and calculated from Sosinsky and Sommerville equation, Eq. [7] are compared in Figure 5. From Figures 4 and 5, there is no significant change in sulfide capacity due to the changes in TiO₂ content. Although titanium oxide has multivalence nature, of which ionic speciation could be affected by the oxygen potential as well as aluminate structure, it is obvious that TiO₂ has minor impact on sulfide capacity of the present slag system. However, the structural role of titanium oxide in the calcium aluminate-based melts should be investigated by employing the spectroscopic methodology, for example, Raman spectroscopy,^[25] which is beyond the scope of the present study. On the other hand, the sulfide capacity continuously increases as the CaO/Al₂O₃ ratio increases. The scatters in three kinds of estimations are not significant and thus the sulfide capacity calculations from measured results in the present study are within the acceptable window.

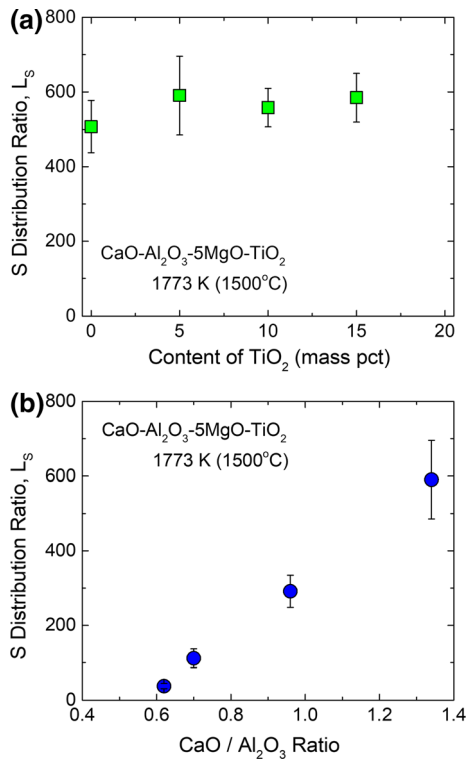


Fig. 6—Equilibrium sulfur distribution ratio as a function of (a) TiO_2 content and (b) $\text{CaO}/\text{Al}_2\text{O}_3$ ratio of the $\text{CaO}-\text{Al}_2\text{O}_3-5$ pct $\text{MgO}-\text{TiO}_2$ slag at 1773 K (1500 °C).

The measured sulfur distribution ratios between Incoloy[®] 825 superalloy and slag, L_s at 1773 K (1500 °C) are represented in Figure 6. As similar to the sulfide capacity, there is no significant deviation in L_s by varying TiO_2 content to 15 mass pct, whereas L_s significantly increases from approx. $L_s = 40$ to 570 as C/A ratio increases from C/A = 0.6 to 1.3. By employing the thermodynamic behavior of sulfur between Incoloy[®] 825 superalloy and the $\text{CaO}-\text{Al}_2\text{O}_3-5$ pct $\text{MgO}-\text{TiO}_2$ slag, the kinetics of sulfur removal from Incoloy[®] 825 superalloy melt will be quantitatively discussed in the following section.

B. Desulfurization Kinetics of Incoloy[®] 825 Superalloy via Various Slag Compositions

Sulfur concentration in Incoloy[®] 825 superalloy melt through fully liquid slag with reaction time is shown in Figure 7 for various slag compositions such as TiO_2 content [Figure 7(a)] and $\text{CaO}/\text{Al}_2\text{O}_3$ ratio [Figure 7(b)]. In our previous studies in molten steel, it was confirmed that the sulfur concentration approaches the equilibrium value within 10 to 15 minutes.^[36,37] However, in the present study, the sulfur concentration rapidly decreases within 20 to 30 minutes. As shown in Figure 7(a), there is no considerable difference in desulfurization rate according to the change in the TiO_2 content, whereas the desulfurization rate is significantly affected by the C/A ratio as shown in Figure 7(b).

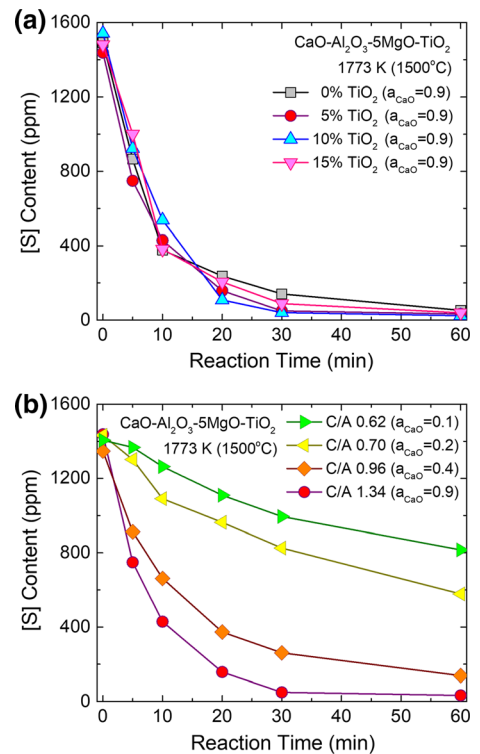


Fig. 7—Changes of sulfur concentration in Incoloy[®] 825 superalloy melt as a function of reaction time for various (a) TiO_2 contents and (b) $\text{CaO}/\text{Al}_2\text{O}_3$ ratios at 1773 K (1500 °C).

It has been proposed that the overall desulfurization rate in secondary refining processes is mainly controlled by mass transfer of sulfur in metal phase due to the relatively high slag basicity, *i.e.*, high sulfide capacity as well as rapid interfacial chemical reactions at high temperatures.^[38–43] Also, the desulfurization rate equation is generally expressed as 1st-order reaction to sulfur concentration in the metal phase as given in Eqs. [8] and [9].^[38,39,43]

$$-\frac{dC}{dt} = k(C - C_{eq}) \quad [8]$$

$$-\ln\left(\frac{C_t - C_{eq}}{C_0 - C_{eq}}\right) = kt, \quad [9]$$

where C_0 , C_t , k , and t are, respectively, the initial sulfur concentration in liquid metal at time $t=0$, the S concentration at time $t = t$, the apparent 1st-order rate constant (s^{-1}), and the reaction time (s). The apparent rate constant, k calculated from Eq. [9] is shown as a function of TiO_2 content and C/A ratio of the slag in Figure 8. The apparent rate constant does not vary by TiO_2 content, while it is strongly affected by C/A ratio of the slag. Specifically, the apparent rate constant sharply decreases by decreasing the C/A ratio at C/A < 1.0 regime.

For sulfur mass transfer, flux through the metal and slag phases can be expressed as follows:^[43]

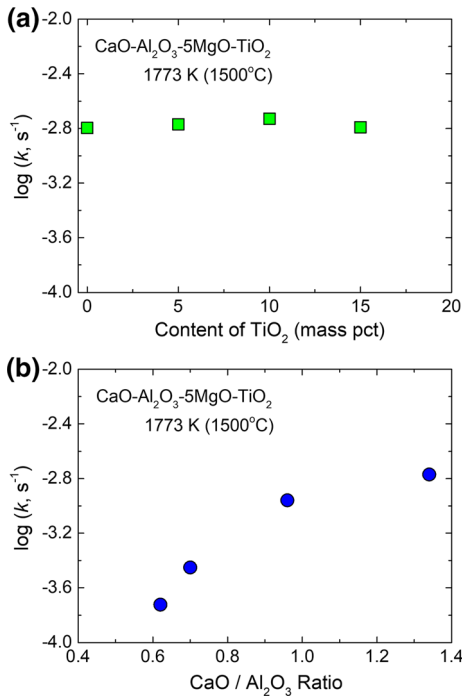


Fig. 8—Apparent rate constant estimated from the 1st-order reaction for various (a) TiO₂ contents and (b) CaO/Al₂O₃ ratios of the slag at 1773 K (1500 °C).

$$J_m = -\frac{dC V_m}{dt A} = k_m (C_m^b - C_m^i) \quad [10]$$

$$J_s = -\frac{dC V_s}{dt A} = k_s (C_s^i - C_s^b). \quad [11]$$

Under the steady state conditions, *i.e.*, $J_m = J_s$, the overall desulfurization flux (J) and overall mass transfer coefficient (k_O) values can be deduced in Eqs. [12] and [13] below:

$$J = k_O \left(C_m^b - \frac{C_s^b}{L_S} \right) \quad [12]$$

$$k_O = \frac{1}{\frac{1}{k_m} + \frac{\rho_m}{\rho_s k_s L_S}}, \quad [13]$$

where J , C , V , A , k_O , t , and ρ , respectively, represent the molar flux of sulfur (mol m⁻² s⁻¹), the molar concentration of sulfur (mol m⁻³), the volume (m³), the reaction area (m²), the overall mass transfer coefficient (m s⁻¹), time (sec), and density (kg m⁻³). Superscripts b and i indicate the bulk and interface, while subscripts m and s indicate the metal and slag phase, respectively. If the desulfurization rate can be determined through mixed mass transfer in the metal and slag phases both, the slag-metal reaction can be regarded as a coupled reaction without prioritization to either metal phase control or slag phase control as the rate-controlling step (RCS). Therefore, the overall mass transfer

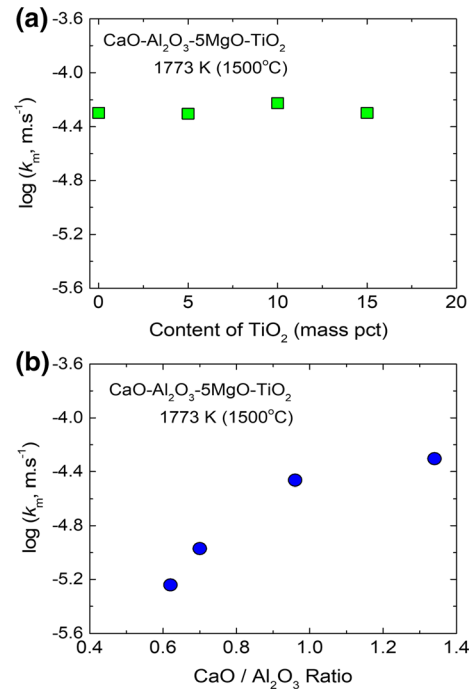


Fig. 9—Relationship between the mass transfer coefficient in metal phase k_m and the (a) TiO₂ contents and (b) CaO/Al₂O₃ ratios of the slag at 1773 K (1500 °C).

coefficient can be represented in Eq. [13]. The denominator in Eq. [13] can be considered as the total resistance to mass transfer, where $\frac{\rho_m}{\rho_s k_s L_S}$ is the resistance in the slag phase and $\frac{1}{k_m}$ is the resistance in the metal phase. Thus, the overall mass transfer coefficient can be deduced by either k_m or $k_s L_S \frac{\rho_s}{\rho_m}$ depending on the variation in mass transfer coefficients between the metal and slag phase, and/or the value of L_S .

By integrating Eqs. [10] and [11], the following rate formulas in Eqs. [14] and [15] could be deduced:

$$-\left(\frac{W_m}{\rho_m A}\right) \left(\frac{[S]_0 - [S]_e}{[S]_o}\right) \ln\left(\frac{[S]_t - [S]_e}{[S]_o - [S]_e}\right) = k_m t \quad [14]$$

$$-\left(\frac{W_s}{\rho_s A}\right) \left(\frac{[S]_e}{[S]_o}\right) \ln\left(\frac{[S]_t - [S]_e}{[S]_o - [S]_e}\right) = k_s t, \quad [15]$$

where W and $[S]$ represent the weight (kg) and S concentration in the metal phase (mass pct), respectively. The subscripts o and e represent initial ($t = 0$) and equilibrium ($t = t_{eq}$) conditions, respectively. The metal phase mass transfer coefficient, k_m , according to the slag compositions are shown in Figure 9. Despite the increase of TiO₂ in the slag, k_m showed almost constant value, whereas k_m significantly decreases as C/A ratio decreases at C/A < 1.0. This indicates that TiO₂ does not affect the desulfurization mechanism in metal phase mass transfer-controlled regime, while the transition of RCS occurs from metal phase mass transfer to slag phase mass transfer or mixed-controlled regime as decreasing C/A ratio at C/A < 1.0.

The relationship between the overall mass transfer coefficient, k_O (obtained from Eq. [13]) and the sulfide capacity as well as viscosity of the slag are shown in Figure 10. In Figure 10(a), the overall mass transfer coefficient k_O linearly increases with increasing sulfide capacity of the slag on a logarithmic scale. In addition, the viscosity of the slag was calculated using FactSageTM7.3 software. As shown in Figure 10(b), the viscosity (η) does not affect the k_O value at $\eta < 2$ dPa s (poise), while k_O significantly decreases with the increase in viscosity of the slag at $\eta > 2$ dPa s.

Meanwhile, the slag phase mass transfer coefficient k_s can be expressed as the following Eq. [16]^[41–43]:

$$k_s = \frac{D}{\delta}, \quad [16]$$

where D and δ , respectively, represent the diffusion coefficient ($\text{m}^2 \text{s}^{-1}$) and diffusion boundary layer (m). Here, the diffusion coefficient of sulfur D can be expressed as follows according to the Stokes–Einstein equation [17].^[44]

$$D = \frac{k_B T}{6\pi\eta r}, \quad [17]$$

where k_B is Boltzmann’s constant ($1.38 \times 10^{-23} \text{ J K}^{-1}$), T is temperature (K), η is the viscosity of slag (dPa s), and r is the radius of the spherical particle (m). From

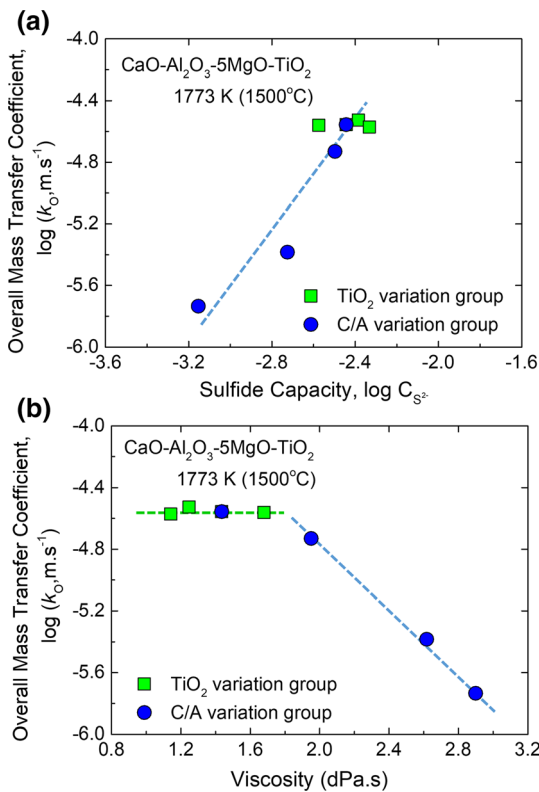


Fig. 10—Overall mass transfer coefficient as a function of (a) sulfide capacity and (b) viscosity of the slag at 1773 K (1500 °C).

Eq. [17], diffusion coefficient of sulfur D is inversely proportional to slag viscosity at a given temperature, which means that the slag phase mass transfer coefficient k_s are also inversely affected by slag viscosity from Eqs. [16] and [17].

Jeong *et al.*^[37] investigated the characteristics of slag by considering the thermochemical and thermophysical properties of slag, *i.e.*, ‘ $\log C_{S_2} - \log \eta$ ’ to evaluate the mass transfer coefficient of sulfur in the desulfurization process of molten steel. In the present study, one more thermodynamic parameter, a_O (the activity of oxygen in the Incoloy[®] 825 superalloy) is employed, resulting in the ‘ $\log C_s - \log \eta - \log a_O$,’ because the distribution ratio of sulfur, L_s , which is one of the dominant factors affecting the overall mass transfer coefficient from Eq. [13], is dependent on the activity of oxygen in the molten alloy as given in Eq. [3]. The overall mass transfer coefficient $\log k_O$ is plotted as a function of physicochemical parameter ‘ $\log C_s - \log \eta - \log a_O$ ’ in Figure 11, wherein a good linear relationship can be obtained with the following equation from a least square regression method.

$$\log k_O = 0.60(\pm 0.05)\{\log C_s - \log \eta - \log a_O\} - 6.1(\pm 0.1), (r^2 = 0.96) \quad [18]$$

From this linear relationship, the thermochemical properties such as sulfide capacity of slag as well as the activity of oxygen in molten alloy in conjunction with the thermophysical property such as slag viscosity are combinatorial factors controlling sulfur removal mechanism.

The relationship between the equilibrium sulfur distribution ratio and the overall mass transfer coefficient is presented in Figure 12. Solid circles represent the current experimental results (*i.e.*, the overall mass transfer coefficient, k_O , calculated from Eq. [13]), and black solid line represents the metal phase mass transfer coefficient measured in the present study ($\log k_m = -4.3$). Open triangles and a grey dashed line were obtained from Kang *et al.*’s study,^[36] in which the desulfurization experiments were performed on steel melt under the similar conditions to that of present study, *i.e.*, the same dimension of crucible assembly with

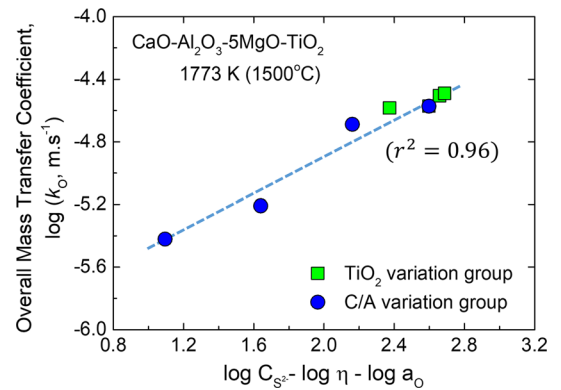


Fig. 11—Overall mass transfer coefficient as a function of physicochemical parameter, $\log C_s - \log \eta - \log a_O$ at 1773 K (1500 °C).

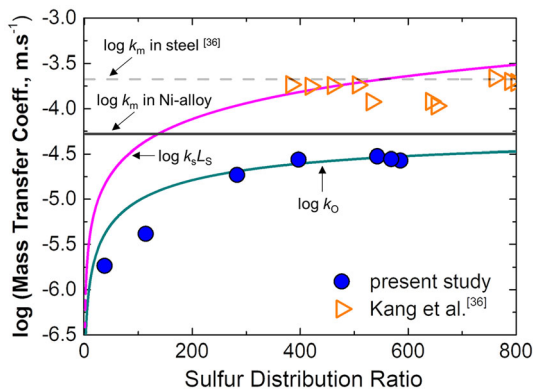


Fig. 12—Relationship between the mass transfer coefficients of sulfur and equilibrium sulfur distribution ratio in the molten Ni-based alloy. The metal phase mass transfer coefficient of sulfur in molten steel is also compared^[36]

same slag/metal ratio ($=0.1$) using an identical induction furnace, and similar CaO-Al₂O₃-MgO-based slag system. A different condition is temperature: Kang *et al.*^[36] performed desulfurization experiment at 1823 K (1550 °C). Thus, their experimental data were extrapolated to 1773 K (1500 °C) from an Arrhenius equation (i.e., activation energy) they reported.

Kang *et al.*^[36] concluded that the overall desulfurization rate was determined by the mass transfer of sulfur in the metal phase when the equilibrium S distribution ratio is higher than about $L_S = 200$ and deduced the metal phase mass transfer coefficient to be $k_m = 2.0 \times 10^{-4}$ m/s ($\log k_m = -3.7$), which is four times higher than the metal phase mass transfer coefficient in Ni-based alloy melt. From Figure 12, the overall mass transfer coefficient ($\log k_o$) drastically decrease by decreasing the equilibrium S distribution ratio. The overall mass transfer coefficient, k_o , approaches gradually to the metal phase mass transfer coefficient, k_m , under condition for the higher equilibrium S distribution ratio, i.e., $L_S > 200$. However, the overall mass transfer coefficient rapidly converges to the $k_s \cdot L_S$ under the condition for the lower S distribution ratio, specifically $L_S < 200$.

C. Difference of Desulfurization Rate in Iron- and Nickel-Based Melts

As mentioned in the previous section, the present study for Ni-based alloy melts and Kang *et al.*'s work for molten steel showed a large difference in desulfurization rate, despite almost similar experimental conditions except for the difference in base metal system. From Eq. [17], the reason for the difference in the metal phase mass transfer coefficient, k_m is possibly caused by the difference in the diffusivity of sulfur in iron- or nickel-based alloy melts. Because the same apparatus and the similar experimental conditions were adopted in both studies, the diffusion boundary layer thickness (δ) can be assumed to be similar in both studies. This can be

indirectly corroborated by the similar convective flow of the melt due to an induction heating with the same frequency in all experiments.

Frazier *et al.*^[45] reported the diffusion coefficient of sulfur in nickel from 1300 K to 1750 K (1027 °C to 1477 °C). From an extrapolation of Frazier *et al.*'s results to 1773 K to 1823 K (1500 °C to 1550 °C), the diffusion coefficient of sulfur in nickel was deduced as $D_S^{\text{Ni}} = 5.08 \times 10^{-11}$ m² s⁻¹ (1773 K [1500 °C]) to $D_S^{\text{Ni}} = 7.63 \times 10^{-11}$ m² s⁻¹ (1823 K [1550 °C]), respectively, which is about 1/60 to 1/90 of sulfur diffusion coefficient in iron, i.e., $D_S^{\text{Fe}} = 4.5 \times 10^{-9}$ m² s⁻¹ at 1823 K (1550 °C). Thus, it is certain that the diffusion coefficient of sulfur in nickel is much less than that in molten iron considering a similarity of density and viscosity of molten nickel and iron as given in Table V. Nevertheless, further research is needed to reveal a difference in the diffusion kinetics of sulfur between iron- and nickel-based melts.

IV. CONCLUSIONS

In the present study, desulfurization behavior of Ni-based superalloy (Incoloy[®] 825 superalloy) melts with the CaO-Al₂O₃-MgO-TiO₂ slag with different content of TiO₂ and CaO/Al₂O₃ ($=C/A$) ratio at 1773 K (1500 °C) was investigated. Moreover, the rate-controlling step of the desulfurization in the present refining process and the transition of the rate-controlling step via slag conditions were discussed. The following is a summary of the major findings reported in the present study:

1. Sulfide capacity of the slag was not changed dramatically with different TiO₂ contents, while it was drastically decreased by decreasing C/A ratio. There was good correspondence between the calculated results by using FactSageTM7.3 software or using optical basicity model, and obtained results from measured sulfur distribution ratio in the present experiment.
2. The metal phase mass transfer controlled regime was not affected by the changes in TiO₂ content of the slag near the CaO saturation composition range. However, when the CaO/Al₂O₃ ratio is lower than unity, in which a sulfur distribution ratio is lower than 200, the transition of RCS from the metal phase mass transfer to the slag phase mass transfer or slag-metal combined transportation-controlled regime was observed.
3. There was a difference in the desulfurization rate in nickel-based (superalloy) and iron-based (steel) melts under the similar refining conditions. This seems to be caused by the difference in a diffusivity of sulfur in Ni-based and Fe-based melts, but further research needs to be performed to reveal the quantitative analysis.

Table V. Diffusion Coefficient of Sulfur in Ni- and Iron-based Melts

Metal System	Diffusion Coefficient of S (m ² /s)	Density (kg/m ³) ^[47]	Viscosity (mPa s) ^[48]
Pure Ni	5.08×10 ⁻¹¹ (extrapolated to 1773 K) ^[45]	7840 (1773 K)	4.4 (1773 K)
	7.63×10 ⁻¹¹ (extrapolated to 1823 K) ^[45]	7800 (1823 K)	4.1 (1823 K)
Pure Fe	4.5×10 ⁻⁹ (1823 K) ^[46]	7030 (1823 K)	5.8 (1823 K)

ACKNOWLEDGMENTS

This work was supported by the Competency Development Program for Industry Specialists from the Korea Institute for Advancement of Technology (KIAT, Grant Number P0002019) and the Korea Evaluation Institute of Industrial Technology (KEIT, Grant Number 20009956), funded by the Ministry of Trade, Industry and Energy (MOTIE), Korea. Also, this study was partly supported by the LG Yonam Foundation, Korea.

FUNDING

Open access funding provided by Royal Institute of Technology.

CONFLICT OF INTEREST

On behalf of all authors, the corresponding author states that there is no conflict of interest.

OPEN ACCESS

This article is licensed under a Creative Commons Attribution 4.0 International License, which permits use, sharing, adaptation, distribution and reproduction in any medium or format, as long as you give appropriate credit to the original author(s) and the source, provide a link to the Creative Commons licence, and indicate if changes were made. The images or other third party material in this article are included in the article's Creative Commons licence, unless indicated otherwise in a credit line to the material. If material is not included in the article's Creative Commons licence and your intended use is not permitted by statutory regulation or exceeds the permitted use, you will need to obtain permission directly from the copyright holder. To view a copy of this licence, visit <http://creativecommons.org/licenses/by/4.0/>.

REFERENCES

1. W.R. Sun, S.R. Guo, J.H. Lee, N.K. Park, Y.S. Yoo, S.J. Choe, and Z.Q. Hu: *Mater. Sci. Eng. A*, 1998, vol. 247, pp. 173–79.
2. J.X. Dong, X.S. Xie, and R.G. Thompson: *Metall. Mater. Trans. A*, 2000, vol. 31A, pp. 2135–44.
3. J.P. Beckman and D.A. Woodford: *Proc. of Superalloys 1988*, The Metallurgical Society, 1988, pp. 795–804.
4. G.A. Meyer, J.S. Warner, Y.K. Rao, and H.H. Kellogg: *Metall. Trans. B*, 1975, vol. 6B, pp. 229–35.
5. G.K. Sigworth, J.F. Elliott, G. Vaughn, and G.H. Geiger: *Trans. Metall. Soc. CIM*, 1977, pp. 104–10.
6. R.Y. Lin, D.C. Hu, and Y.A. Chang: *Metall. Trans. A*, 1978, vol. 9B, pp. 531–38.
7. S. Utada, Y. Joh, M. Osawa, T. Yokokawa, T. Kobayashi, K. Kawagishi, S. Suzuki, and H. Harada: *Proc. of Superalloys 2016, TMS*, 2016, pp. 591–99.
8. T. Degawa and T. Ototani: *Tetsu-to-Hagane*, 1987, vol. 73, pp. 1691–97.
9. Y. Kishimoto, S. Utada, T. Iguchi, Y. Mori, M. Osawa, T. Yokokawa, T. Kobayashi, K. Kawagishi, S. Suzuki, and H. Harada: *Metall. Mater. Trans. B*, 2020, vol. 51B, pp. 293–305.
10. Y. Kishimoto, T. Kono, T. Horie, T. Yokokawa, M. Osawa, K. Kawagishi, S. Suzuki, and H. Harada: *Metall. Mater. Trans. B*, 2021, vol. 52B, pp. 1450–62.
11. T. Zhang, Y. Wei, J. Chen, N. Li, and B. Han: *J. Aust. Ceram. Soc.*, 2020, vol. 56, pp. 885–94.
12. J. Niu and Z. Hu: *Adv. Mater. Res.*, 2011, vols. 284–286, pp. 2433–36.
13. R.C. Reed: *The Superalloys-Fundamentals and Applications*, Cambridge University Press, Cambridge, 2006, pp. 217–29.
14. M. Eissa and A. El-Mohammadi: *Steel Res.*, 1998, vol. 69, pp. 413–17.
15. J.G. Yang and J.H. Park: *Metall. Mater. Trans. B*, 2017, vol. 48B, pp. 2147–56.
16. S.C. Duan, X. Shi, F. Wang, M.C. Zhang, B. Li, W.S. Yang, H.J. Guo, and J. Guo: *J. Mater. Res. Technol.*, 2019, vol. 8, pp. 2508–16.
17. H.E.O. Kellner, A.V. Karasev, A. Memarpour, and P.G. Jonsson: *Steel Res. Int.*, 2016, vol. 87, pp. 1461–68.
18. J.H. Cho, J. Martinsson, D. Sichen, and J.H. Park: *to be published*.
19. J.A. Rotole, K. Gaskell, A. Comte, and P.M.A. Sherwood: *J. Vac. Sci. Technol. A*, 2001, vol. 19, pp. 1178–81.
20. www.factsage.com. Accessed April 2021.
21. C.W. Bale, E. Belisle, S.A. Decterov, G. Eriksson, K. Hack, I.H. Jung, Y.B. Kang, J. Melancon, A.D. Pelton, C. Robelin, and S. Petersen: *Calphad*, 2009, vol. 33, pp. 295–311.
22. J.H. Park: *J. Non-Cryst. Solids*, 2012, vol. 358, pp. 3096–3102.
23. J.S. Park and J.H. Park: *Steel Res. Int.*, 2014, vol. 85, pp. 1303–09.
24. J.H. Park, I.H. Jung, and S.B. Lee: *Met. Mater. Int.*, 2009, vol. 15, pp. 677–81.
25. Y.B. Kang and J.H. Park: *Metall. Mater. Trans. B*, 2011, vol. 42B, pp. 1211–17.
26. J.H. Heo, S.S. Park, and J.H. Park: *Metall. Mater. Trans. B*, 2012, vol. 43B, pp. 1098–1105.
27. J.H. Park: *Calphad*, 2007, vol. 31, pp. 149–54.
28. S.K. Kwon, Y.M. Kong, and J.H. Park: *Met. Mater. Int.*, 2014, vol. 20, pp. 959–66.
29. J.H. Park, G.H. Park, and Y.E. Lee: *ISIJ Int.*, 2010, vol. 50, pp. 1078–83.
30. J.H. Shin and J.H. Park: *Metall. Mater. Trans. B*, 2017, vol. 48B, pp. 2820–25.
31. J.H. Park: *J. Am. Ceram. Soc.*, 2006, vol. 89, pp. 608–15.
32. J.A. Duffy and M.D. Ingram: *J. Am. Chem. Soc.*, 1971, vol. 93, pp. 6448–54.
33. J.A. Duffy: *J. Non-Cryst. Solids*, 1989, vol. 109, pp. 35–39.
34. J.A. Duffy: *J. Chem. Educ.*, 1996, vol. 73, pp. 1138–42.
35. D.J. Sosinsky and I.D. Sommerville: *Metall. Trans. B*, 1986, vol. 17B, pp. 331–37.
36. J.G. Kang, J.H. Shin, Y.S. Chung, and J.H. Park: *Metall. Mater. Trans. B*, 2017, vol. 48B, pp. 2123–35.
37. T.S. Jeong and J.H. Park: *Metall. Mater. Trans. B*, 2020, vol. 51B, pp. 2309–19.
38. F. Oeters: *Metallurgie der Stahlherstellung*, Verlag Stahleisen GmbH, Dusseldorf, and Springer, Berlin, 1994.

39. J.X. Deng and F. Oeters: *Proc. 7th Japan-Germany Seminar on Fundamentals of Iron and Steelmaking*, Verlag Stahleisen GmbH, Dusseldorf, 1987, p. 33.
40. Y.H. Kim: Ph.D. Dissertation, University of Strathclyde, Strathclyde, Glasgow, UK, 1978.
41. B. Deo and P. Grieveson: *Steel Res.*, 1986, vol. 57, pp. 514–19.
42. S. Ramachandran, T.B. King, and N.J. Grant: *Trans. Metall. Soc. AIME*, 1956, vol. 206, pp. 1549–53.
43. B. Deo and R. Boom: *Fundamentals of Steelmaking Metallurgy*, Prentice Hall, New York, 1993.
44. A. Einstein: *Ann. Phys.*, 1905, vol. 17, pp. 549–60.
45. W.E. Frazier, T.T. Mickle, and B.A. Pregger: Research Report, Naval Air Development Center, Department of The Navy, 1993.
46. T. Saito, Y. Kawai, K. Maruya, and M. Maki: *Sci. Rep. Inst. Tohoku Univ. Ser. A*, 1959, vol. 11, pp. 401–10.
47. M. Watanabe, M. Adachi, and H. Fukuyama: *J. Mater. Sci.*, 2016, vol. 51, pp. 3303–10.
48. Y. Sato, K. Sugisawa, D. Aooki, and T. Yamamura: *Meas. Sci. Technol.*, 2005, vol. 16, pp. 363–71.

Publisher's Note Springer Nature remains neutral with regard to jurisdictional claims in published maps and institutional affiliations.